BeBeC-2018-S04

INVERSE METHODS FOR THREE-DIMENSIONAL ACOUSTIC MAPPING WITH A SINGLE PLANAR ARRAY

Gianmarco Battista[1], Paolo Chiariotti[1], Gert Herold[2], Ennes Sarradj[2], Paolo Castellini[1]
[1]Università Politecnica delle Marche
Via Brecce Bianche, 60131, Ancona, Italy
[2]Technische Universität Berlin
Einsteinufer 25, D-10587 Berlin, Germany

Abstract

The aeroacoustic source localization task usually involves planar microphone arrays and calculation points located on a surface at a certain distance with respect to the array. An implicit assumption that sources are located on this surface is therefore performed. However, in many cases, this assumption represents an oversimplification of the problem, given that distance of sources with respect to the array are very often unknown. The goal of this paper is to describe strategies for investigating a volume of potential sources rather than a surface. Indeed, this volumetric approach does not need any *a priori* knowledge of array-to-source potential distances. Since direct beamforming techniques have poor spatial resolution in longitudinal direction, i.e. direction normal to the array plane, more refined algorithms, like deconvolution techniques or inverse methods, are required to obtain useful results. In this work inverse methods (Equivalent Source Method - ESM - and Covariance Matrix Fitting - CMF) are exploited in the context of volumetric noise source imaging using a single planar array. Additional issues have to be faced in volumetric imaging with respect to conventional surface imaging. To prove this concepts, different solution methods are tested on simulated data and on a more challenging setup like an airfoil in an open jet.

1 INTRODUCTION

Acoustic source mapping techniques based on microphone arrays are extensively used for noise source localization and quantification. Very often planar arrays are utilized for this purpose and source mapping is performed on planes or surfaces that are supposed to contain all acoustic sources. However, real sources are not necessarily located there and this might cause misleading results. Indeed, it is interesting for the aeroacoustic community to investigate the extension of common acoustic mapping techniques to volumetric mapping. Sarradj [32, 33] analyzed the

problem for direct beamformers using a single planar array. He pointed out that different steering vector formulations (i.e. different spatial filters) are able to provide either correct location or correct level. In addition, due to poor spatial resolution of conventional beamformers in the third dimension, deconvolution techniques such as Orthogonal Beamforming [35], CLEAN-SC [22] or DAMAS [5, 6, 39] are mandatory to obtain accurate reconstruction of real source distribution. Another possibility is to use inverse methods, e.g. *Equivalent Source Method* - ESM - [27] or *Covariance Matrix Fitting* - CMF - [39]. Padois et al. compared the performances of different techniques in three-dimensional mapping and also studied the effect of using multiple planar arrays simultaneously [23, 24]. Ning et al. [20] used *Compressed sensing* techniques to face three-dimensional mapping problem. This work focuses on the use of inverse methods to perform noise source volumetric mapping using a single planar array and describes some strategies to face additional problems that rise in this challenging context. The paper is organized as follows. A theoretical introduction to the inverse acoustic problem and its extension in volumetric noise source imaging is provided in Section 2. Different approaches and solvers are compared in Section 3 by exploiting both simulated and experimental data. The main conclusions of the work are drawn in Section 4

2 THE VOLUMETRIC INVERSE ACOUSTIC PROBLEM

2.1 Inverse acoustic problem formulation

In acoustic imaging, inverse methods make the direct acoustic problem discrete by considering propagation from sources to measurement locations. This relies on the *Wave Superposition Method* [17] which states that the acoustic field, generated by a complex radiator, can be reproduced as a superposition of fields caused by a set of simpler sources enclosed within the radiator. This makes it possible to define a spatial distribution of elementary sources (e.g. monopoles, dipoles, plane waves ecc.) representing complex sources as a combination of them. In frequency domain, the direct source-receiver propagation problem is linear and can be written, for each frequency, as:

$$\mathbf{G}\mathbf{q} = \mathbf{p}\,, \tag{1}$$

where $\mathbf{q} \in \mathbb{C}^{N\times 1}$ is a complex vector of source strengths on N assumed positions, $\mathbf{p} \in \mathbb{C}^{M\times 1}$ is a vector containing acoustic complex pressures at microphone locations and $\mathbf{G} \in \mathbb{C}^{M\times N}$ is the acoustic transfer matrix. The calculation of $\mathbf{p}$ for a given $\mathbf{q}$ is the *direct acoustic problem* which is a well-determined problem and has unique solution. The *inverse acoustic problem* aims to retrieve the source distribution $\mathbf{q}$ from measurement at microphone locations $\mathbf{p}$. This problem results to be ill-posed in the Hadamard sense [9, 12], i.e. existence, uniqueness and stability of the solution are not guaranteed. Inverse problem formulation can be also expressed as a linear system:

$$\hat{\mathbf{q}} = \mathbf{H}\mathbf{p}\,, \tag{2}$$

where $\hat{\mathbf{q}}$ is the solution for a particular inverse operator $\mathbf{H} \in \mathbb{C}^{N\times M}$. Indeed, as it will be shown ahead in the paper, this latter term can assume different forms depending on the selected solution method or the adopted regularization strategy. A complete review about different inverse operators is provided by Leclere et al. in [19].
When the acoustic field is stationary, the former problem can be rearranged in terms of Auto-

and Cross- Power Spectra averaged over several observations:

$$\mathbf{G}\mathbf{Q}\mathbf{G}^H = \mathbf{P}\,, \tag{3}$$

where the superscript ^{H} stands for the complex conjugate transpose operator. The matrix $\mathbf{P} = \langle \mathbf{p}\mathbf{p}^H \rangle$ is the Cross Spectral Matrix - CSM - of pressure at microphone locations and $\mathbf{Q} = \langle \mathbf{q}\mathbf{q}^H \rangle$ is the CSM of sources strengths ($\langle \cdot \rangle$ is the average operator). Using the quadratic form, the solution of the inverse problem can be obtained as

$$\hat{\mathbf{Q}} = \mathbf{H}\mathbf{P}\mathbf{H}^H\,. \tag{4}$$

The main advantage of inverse methods with respect to classic direct beamforming approach is that all sources are considered together, thus leading to better results in terms of source strength quantification and in presence of multiple correlated/uncorrelated acoustic sources. However, since the number of equivalent sources is usually much greater than the number of microphones, the problem is generally under determined.
A straightforward approach for solving Eq. 1 can be identified in the *Moore-Penrose pseudo-inverse*, which is a generalization of inverse matrix to rectangular matrices. Since the linear system is under determined an exact solution is provided by the right pseudo-inverse. This inverse operator returns the *Least 2-Norm Solution*, i.e. the solution with the smallest 2-norm among those satisfying the linear equations in Eq. 1 :

$$\mathbf{H} = \mathbf{G}^{+R} = \mathbf{G}^H(\mathbf{G}\mathbf{G}^H)^{-1}\,, \tag{5}$$

$$\hat{\mathbf{q}} = \mathbf{G}^{+R}\mathbf{p} \;= \arg\min_{\mathbf{q}} \left(\|\mathbf{q}\|_2^2 \text{ subject to } \mathbf{G}\mathbf{q} = \mathbf{p} \right)\,. \tag{6}$$

From a physical point of view, this represents the minimum energy solution that exactly matches the pressure data measured. This is often referred to as *naïve solution*. However, even though the pseudo-inverse approach is supposed to provide a unique and exact solution, the latter may still be unstable because of errors in the propagation model and/or noise in measured data (providing variations on $\mathbf{G}$ and $\mathbf{p}$ respectively). The *Discrete Picard Condition* - DPC - [10] might help in addressing this stability issue. Indeed, a given right-hand term $\mathbf{p}$ of Eq. 1 satisfies the DPC if, for all numerically non-zero singular values s_i (extracted via a Singular Value Decomposition - SVD - of the $\mathbf{G}$ operator), the corresponding Fourier coefficients $\mathbf{u}_i^H\mathbf{p}$, being $\mathbf{u}_i$ the columns of the $\mathbf{U} \in \mathbb{C}^{M\times M}$ unitary matrix extracted from the SVD of $\mathbf{G}$, decay to zero faster than s_i on the average. This means that, once defined the terms η_i as

$$\eta_i = \frac{|\mathbf{u}_i^H\mathbf{p}|}{s_i}, \tag{7}$$

named here *Picard coefficients*, the solution is stable if η_i are constant, or decreasing, on the average. This condition can be checked by visual inspection of a *Picard plot*, which shows the trend of Picard coefficients. Noise has an effect on the Fourier coefficients, in particular those related to the smallest singular values, and is amplified during the inversion thus making the solution unstable.

A common approach to lower this amplification effect is to exploit the *Tikhonov regularization* [38]. The Tikhonov approach consists in jointly minimizing the solution norm $\|\mathbf{q}\|_2^2$ and

residuals norm $\|\mathbf{Gq}-\mathbf{p}\|_2^2$, thus leading to the following minimization problem:

$$\hat{\mathbf{q}}(\lambda) = \arg\min_{\mathbf{q}} \left(\|\mathbf{Gq}-\mathbf{p}\|_2^2 + \lambda^2 \|\mathbf{q}\|_2^2 \right) \tag{8}$$

where the *Regularization parameter* $\lambda^2 \geq 0$ controls the trade-off between the amplitude of the solution and the fitting error.

The regularization parameter amplifies the singular values $s_i < \lambda$ while the singular values $s_i > \lambda$ remain almost unaltered. Therefore, when matrix inversion is performed, the smallest singular values are smoothly filtered preventing the over amplification of noise and stabilizing the solution. In other words, Tikhonov regularization controls the energy of the solution trading this for a small fit error. As the "cut-off" on singular values is adjusted varying λ, the most critical aspect is to estimate the correct regularization parameter for each specific problem. Several strategies are proposed in literature, such as *L-curve criterion* or *Generalized Cross-Validation*, or a combination of them [11],[16],[18].
The general form of Tikhonov regularization makes possible to have more control on the solution considering the following problem:

$$\hat{\mathbf{q}}(\lambda, \mathbf{W}) = \arg\min_{\mathbf{q}} \left(\|\mathbf{Gq}-\mathbf{p}\|_2^2 + \lambda^2 \|\mathbf{Wq}\|_2^2 \right) \tag{9}$$

where the term $\|\mathbf{Wq}\|$ is named discrete smoothing norm. The square invertible matrix $\mathbf{W}$ is used to introduce additional information about the solution. This problem boils down to a standard Tikhonov formulation substituting $\tilde{\mathbf{q}} = \mathbf{Wq}$ and $\tilde{\mathbf{G}} = \mathbf{GW}^{-1}$:

$$\hat{\tilde{\mathbf{q}}}(\lambda, \mathbf{W}) = \arg\min_{\tilde{\mathbf{q}}} \left(\|\tilde{\mathbf{G}}\tilde{\mathbf{q}}-\mathbf{p}\|_2^2 + \lambda^2 \|\tilde{\mathbf{q}}\|_2^2 \right) . \tag{10}$$

The solution of original problem is obtained from $\hat{\mathbf{q}} = \mathbf{W}^{-1}\hat{\tilde{\mathbf{q}}}$.

An alternative, or probably better to say, a generalization of the Tikhonov approach, has been proposed by Antoni some years ago [3]. He exploited Bayesian inference for developing a method that is able to

- identify the optimal basis functions minimizing the reconstruction error;
- include *a priori* information on source distribution to better condition the problem and ease the localization task;
- provide a robust regularization criterion with no more than one minimum.

The Bayesian approach considers experimental errors in a *likelihood functions* which stands for the direct probability of pressures values, given a certain propagation model and the random fluctuations of measurement noise. Indeed, by assuming complex Gaussian *prior probability density function - pdf* for source parameters, the Bayesian framework "mechanically" produces a regularized solution similar to the Tikhonov one. The Bayesian approach, however, identifies the regularization parameter λ^2 in the Noise-to-Signal Ratio - NSR - , i.e. the ratio between noise energy β^2 and source energy α^2 and provides two different strategies for its direct estimation from measured data, namely the *Maximum A Posteriori* - MAP - and the *Joint* approach. For a more detailed explanation on empirical Bayesian regularization in inverse acoustic problem the interested reader might refer to [27, 28].

2.2 Inverse problem solution strategies for volumetric mapping

There are three additional issues when dealing with volumetric mapping:

- high number of potential sources located at very different distances from the array centre;
- poor spatial resolution of the array in the direction moving far away from the array centre;
- high number of potential sources with no contribution to the acoustic field.

One trick to face the first issue is to compensate for the source-receiver distance r. This can be done either exploiting a weighting strategy on the strength-to-pressure acoustic transfer function, as suggested by Pereira et al. [29], or using a pressure-to-pressure acoustic transfer function formulation. In this latter case, when monopoles are considered, the elements of $\mathbf{G}$ are

$$G_{mn} = \frac{r_{0n}}{r_{mn}} e^{-jk(r_{mn}-r_{0n})} \,. \tag{11}$$

This propagator returns the acoustic pressure at microphone location m depending on sound pressure at reference point "0" caused by the monopole source at location n.

It is a well known issue that the direction moving far away from the array centre suffers of poor resolution with respect to the other two, especially when the real source is at a distance greater than one array diameter from the array plane. This aspect may limit localization and quantification accuracy, especially at low Helmholtz numbers - He. One way to overcome this problem is to enforce the sparsity of solution. Indeed this sparsity constraint fits well also with the third item listed above.
Sparsity can be enforced by reformulating the problem in terms of L_p-norm

$$\hat{\mathbf{q}}(\lambda, p) = \arg\min_{\mathbf{q}} \left(\|\mathbf{G}\mathbf{q} - \mathbf{p}\|_2^2 + \lambda^2 \|\mathbf{q}\|_p^p \right) \tag{12}$$

and minimizing for $p < 2$. To obtain accurate solution in volumetric mapping, a value of $0 \leq p \leq 1$ is strongly recommended, even though for $p < 1$ this results in a non-convex optimization problem. The L_0-norm minimization can be approximated by the *Orthogonal Matching Pursuit* [25, 31] algorithm. This is a greedy algorithm that selects only those sources which give the best approximation of measured data. A version of the algorithm making use of cross-validation principle [4] reduces possible reconstruction errors. The L_1-norm minimization can be calculated by means of *Least Angle Regression Lasso* algorithm [37]. Another family of methods raises from Eq. 9, i.e. the general form of Tikhonov regularization. The *Iteratively Reweighted Least Squares* - IRLS - [7, 8] algorithm can be used for obtaining sparse solution and relies on the following consideration:

$$\|\mathbf{q}\|_p^p = \sum_{n=1}^{N} |q_n|^p = \sum_{n=1}^{N} w_n^2 |q_n|^2 = \|\mathbf{W}\mathbf{q}\|_2^2 \,. \tag{13}$$

The weighting matrix $\mathbf{W}$ is a real diagonal matrix and the set of weights depends on the result of the previous iteration according with the following expression:

$$w_n^{(it)} = \left| \hat{q}_n^{(it-1)} \right|^{\frac{(p-2)}{2}} \tag{14}$$

where *it* is the current iteration. This algorithm boils down to an iterative procedure that is a fixed-point for Eq. 12 and converges to global minimum for convex problems ($p \geq 1$) or to a global or local minimum for non-convex problem ($0 \leq p < 1$). As the exponent of weights is negative for $p < 2$, division by 0 must be avoided. For this reason, those equivalent sources, having an amplitude below a threshold, are discarded from calculation. In [21], a threshold of 100 dB with respect to maximum of $|\hat{q}_n|^{(it-1)}$ is suggested. In the same work it is also suggested a convergence criterion:

$$\varepsilon^{(it)} = 10 \log 10 \left(\left\langle \left| \hat{q}_n^{(it)} / \hat{q}_n^{(it-1)} \right| \right\rangle \right) \tag{15}$$

where the operator $\langle \cdot \rangle$ is the spatial average. This criterion requires that source amplitudes remain almost unaltered in the last 2 iterations to stop the algorithm. In this work a slightly different criterion is proposed:

$$\varepsilon^{(it)} = 10 \log 10 \left(MSR - \left| \frac{\mathrm{d}(MSR)}{\mathrm{d}(it)} \right| - \left| \frac{\mathrm{d}^2(MSR)}{\mathrm{d}(it)^2} \right| \right) \tag{16}$$

$$MSR = \left\langle \left| \hat{q}_n^{(it)} / \hat{q}_n^{(it-1)} \right| \right\rangle \tag{17}$$

where MSR stands for *Mean Source Ratio*. This criterion can be evaluated only for $it > 2$ and is more restrictive because it requires that variation in the solution are small over last 3 iteration. The algorithm stops when $\varepsilon^{(it)} \geq -0.1$ dB.

Table 1 shows the solution strategies tested in this work for volumetric acoustic mapping. The *Equivalent Source Method* (ESM) is intended here as a method for solving the linear form of acoustic problem such as the *Generalized Inverse Beamforming* or its variants [27, 30, 36, 40]. A map is calculated for each relevant eigenmode of CSM and then they are summed together to obtain the complete map. Another common approach in literature is the *Covariance Matrix Fitting* (CMF) [14, 15, 39] that means solving the quadratic form of acoustic problem in order to find the combination of sources that produces the "best" fitting of the measured CSM. The assumption of uncorrelated sources is made and therefore source power matrix $\mathbf{Q}$ becomes diagonal. This allows to easily rearrange the quadratic form as a standard linear system and force a real solution. In addition, the linear system is formulated using only the upper triangular part of CSM without the diagonal.

Name	Formulation	Algorithm
ESM-IRLS	Linear	IRLS + Bayesian regularization (MAP)
CMF-OMPCV	Quadratic	Cross-Validated OMP
CMF-LassoLars	Quadratic	LassoLars
CMF-IRLS	Quadratic	IRLS + Bayesian regularization (MAP)

Table 1: Solution strategies

The CMF approach is implemented in the open-source Python software *Acoular* [1, 34] and utilizes the machine learning library *scikit-learn* [26] for Cross-Validated OMP and LassoLars solvers. The latter requires the selection of a regularization parameter λ that represents the trade-off between the fitting error and the L_1 solution norm. The version of IRLS proposed

in this work is implemented in MATLAB and the regularization parameter is estimated using the MAP Bayesian criterion cited above. This solver is applied to CMF and ESM. Since CMF requires positive source coefficients, at each IRLS iteration authors suggest to set positivity constraint to sources having negative power, i.e. force them to 0 as in the Gauss-Seidel procedure of DAMAS.

3 RESULTS

3.1 Simulated data

The first test case is the Analytical Benchmark 8, available at [2]. This dataset represents a simulation of measurements in an open jet wind tunnel with a round jet. Noise sources are three uncorrelated monopoles emitting white noise. Simulated setup is depicted in Fig. 1 where the black circle represents the nozzle of the open jet and black lines mark the region of interest. Source locations are reported using the red crosses. The 64 microphones array is situated above the volume and has an aperture of $D = 1.5$ m. The volume to map has dimensions $D_x = 1$ m, $D_y = 1$ m, $D_z = 0.8$ m and is discretized with three-dimensional regular grid of points using 2 cm of step thus having 106.641 points. The flow is in x-axis direction and the sound propagation through the flow field is calculated using *Acoular* OpenJet environment. The nozzle diameter is 0.5 m and the jet flow speed is 0.2 Mach. Since there are only 3 uncorrelated sources active in the scenario, ESM is applied only to first 3 eigenmodes. The regularization parameter for LassoLars solver is chosen here empirically equals to 10^{-6}. The reconstructed source spectra are obtained by integration of maps over a spherical volume of 6 cm radius centered in the exact source location. Figure 6 depicts the difference in terms of source strength between the exact source spectrum and the one obtained from the map for each tested method.

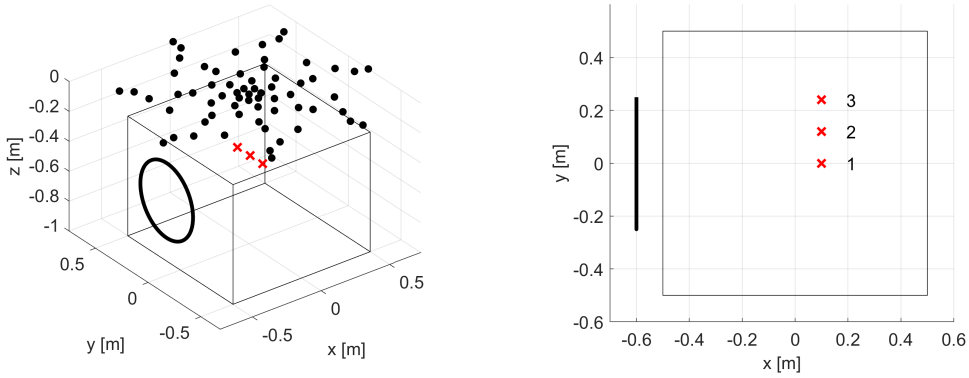

Figure 1: Simulated measurement setup

	x	y	z
Source 1	0.10	0.00	-0.50
Source 2	0.10	0.12	-0.50
Source 3	0.10	0.24	-0.50
Nozzle centre	-0.60	0.00	-0.50

Table 2: Setup coordinates (m)

All methods can correctly localize and separate sources from 2 kHz band onwards (He ≈ 8). Indeed, all maps become similar as frequency increases. However, for lower frequencies only CMF-LassoLars and CMF-IRLS with $p = 0.9$ can recognise three different monopoles. On the contrary, CMF-OMPCV produces a useless solution in this band. Both CMF and ESM solutions obtained using IRLS with $p = 1$ return a sort of single linear source because they are not able to separate different contributes. Lastly, ESM-IRLS with $p = 0.9$ recognizes only two monopoles. Quantification of source spectra is also promising, in particular CMF-based methods provide good estimation from 1.5-2 kHz onwards, while for lower frequencies results strongly depend on the particular solution strategy adopted. Equivalent Source Method starts to provide good estimation of source strength only above 3.5 kHz (He ≈ 14). In general, IRLS based methods show a tendency to slightly underestimate the reconstructed source spectra. The best results,in terms of localization and quantification, are provided by CMF-LassoLars and CMF-IRLS with $p = 0.9$.

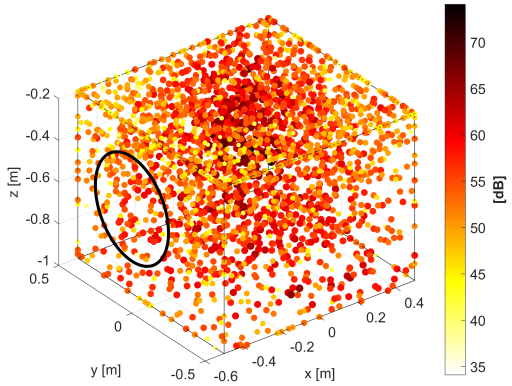

(a) CMF-OMPCV

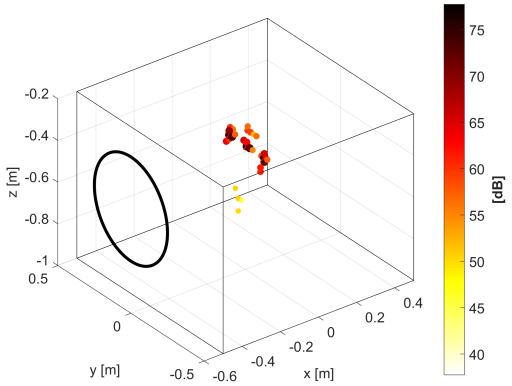

(b) CMF-LassoLars $\lambda = 10^{-6}$

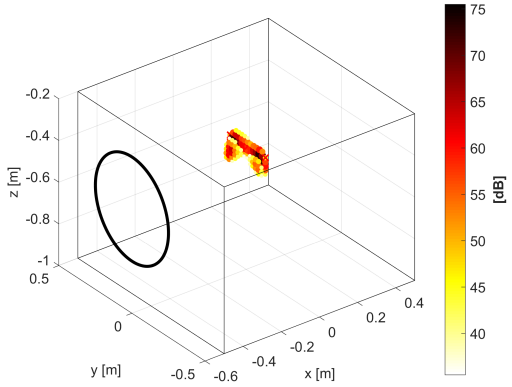

(c) CMF-IRLS $p = 1$

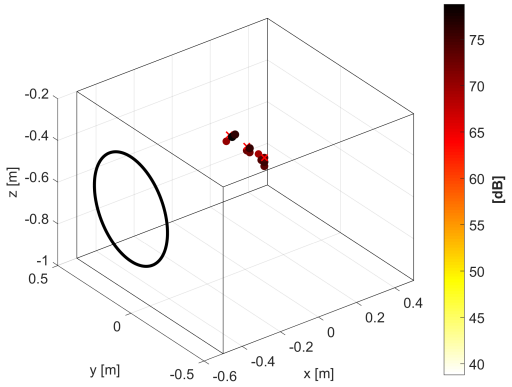

(d) CMF-IRLS $p = 0.9$

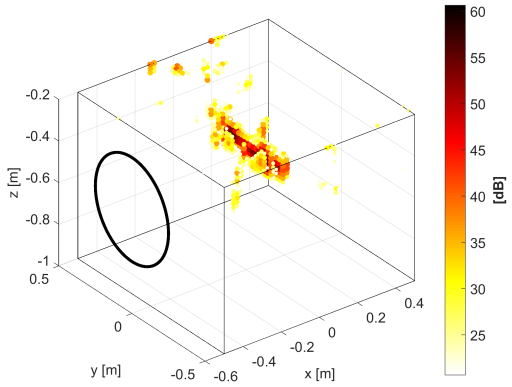

(e) ESM-IRLS $p = 1$

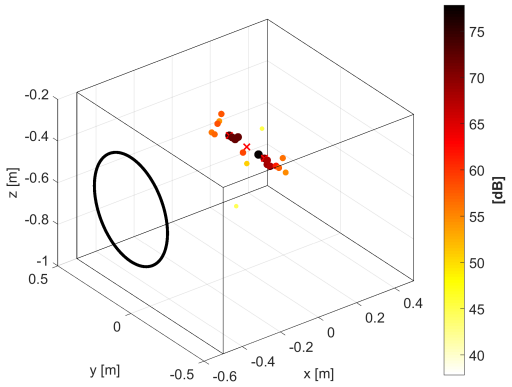

(f) ESM-IRLS $p = 0.9$

Figure 2: 1000 Hz 1/3-octave band (He ≈ 3.8 - 4.7)

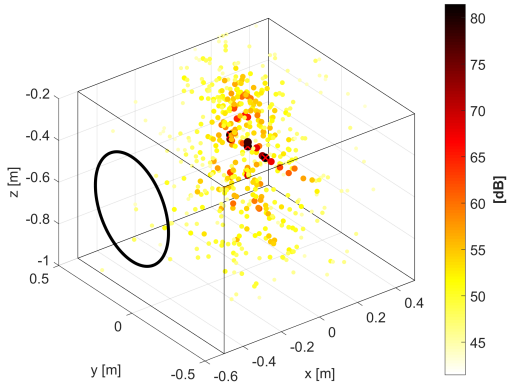

(a) CMF-OMPCV

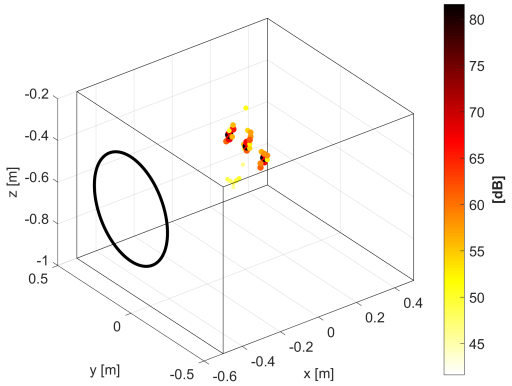

(b) CMF-LassoLars $\lambda = 10^{-6}$

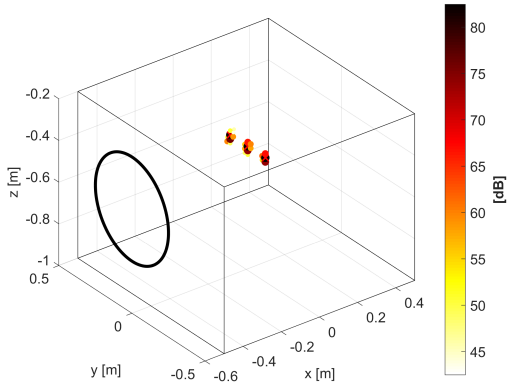

(c) CMF-IRLS $p = 1$

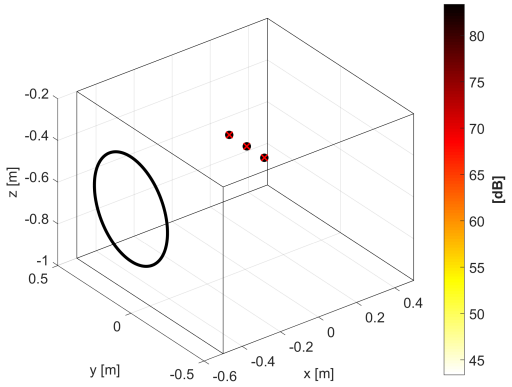

(d) CMF-IRLS $p = 0.9$

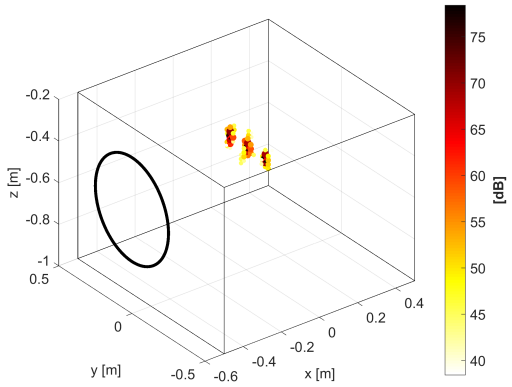

(e) ESM-IRLS $p = 1$

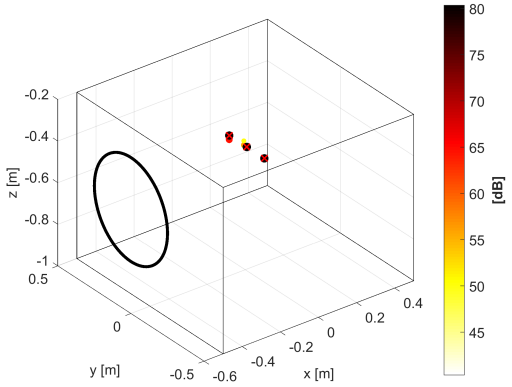

(f) ESM-IRLS $p = 0.9$

Figure 3: 2000 Hz 1/3-octave band (He ≈ 7.6 - 9.4)

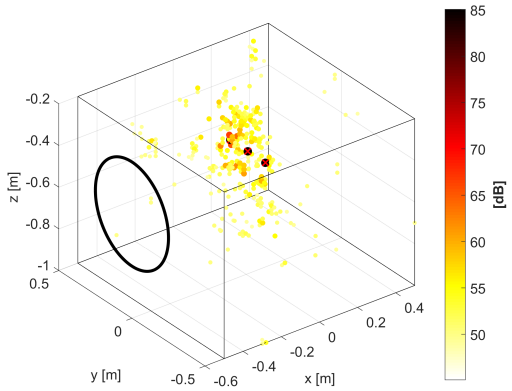

(a) CMF-OMPCV

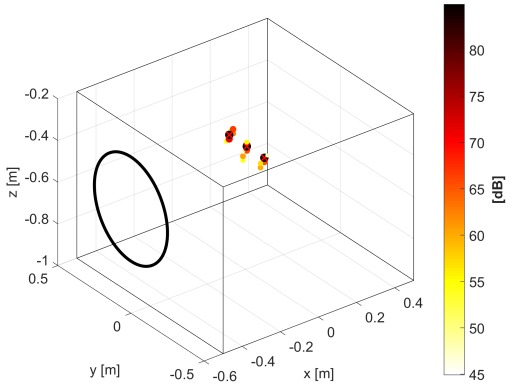

(b) CMF-LassoLars $\lambda = 10^{-6}$

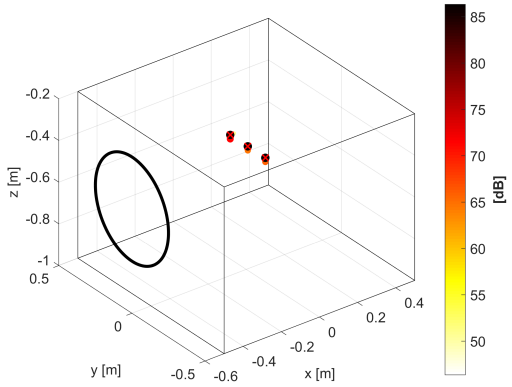

(c) CMF-IRLS $p = 1$

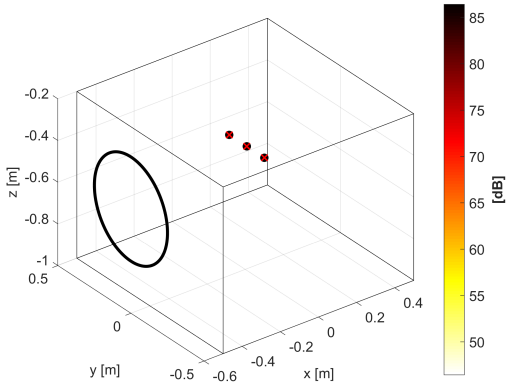

(d) CMF-IRLS $p = 0.9$

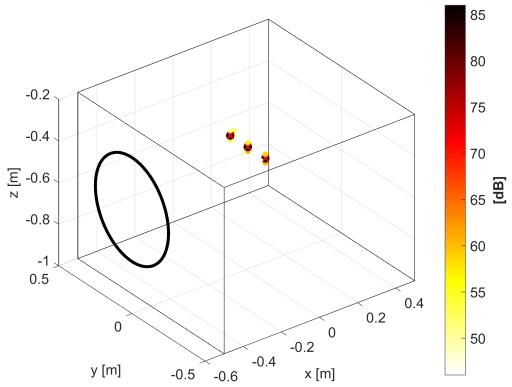

(e) ESM-IRLS $p = 1$

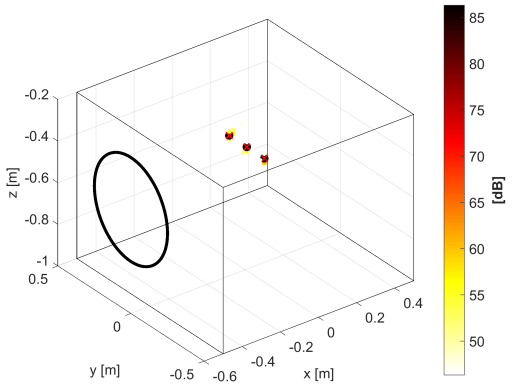

(f) ESM-IRLS $p = 0.9$

Figure 4: 4000 Hz 1/3-octave band (He ≈ 15.3 - 19.0)

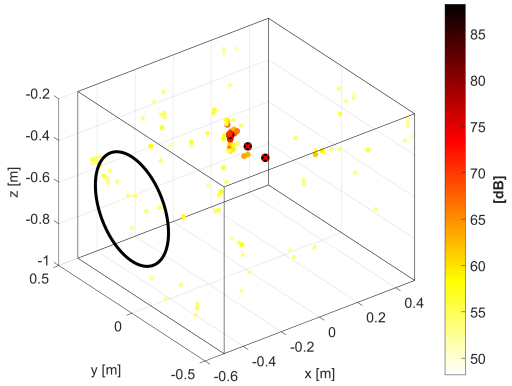

(a) CMF-OMPCV

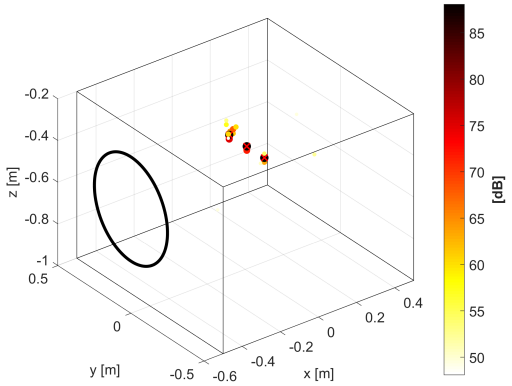

(b) CMF-LassoLars $\lambda = 10^{-6}$

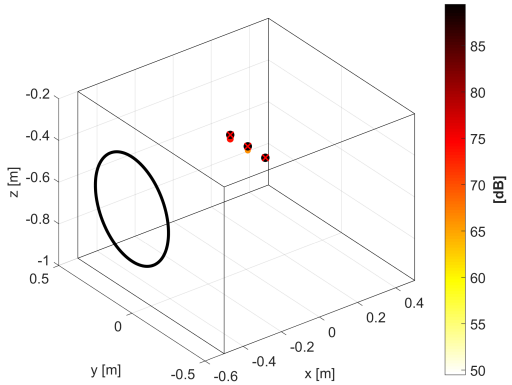

(c) CMF-IRLS $p = 1$

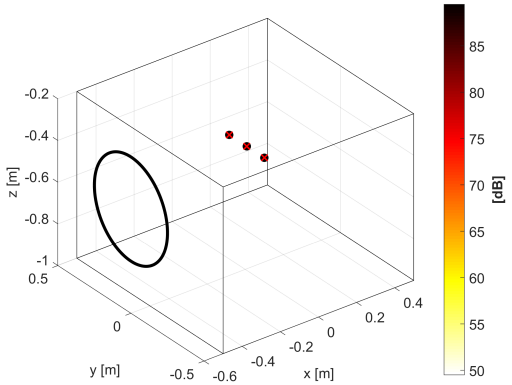

(d) CMF-IRLS $p = 0.9$

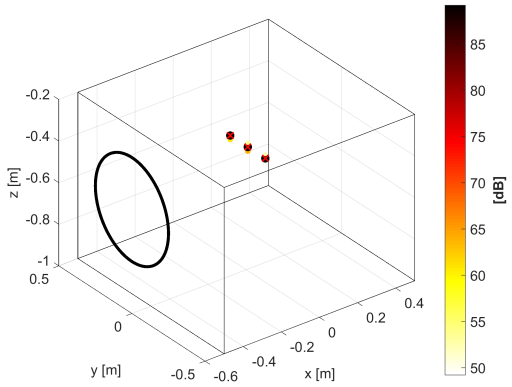

(e) ESM-IRLS $p = 1$

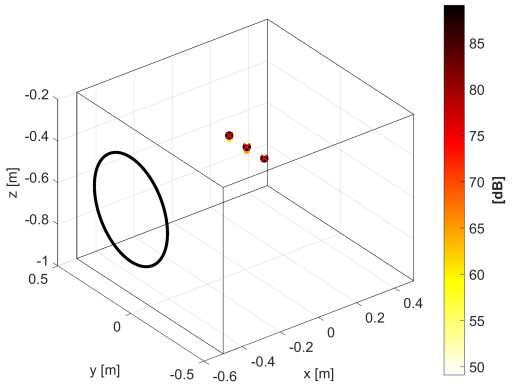

(f) ESM-IRLS $p = 0.9$

Figure 5: 8000 Hz 1/3-octave band (He ≈ 30.5 - 38.2)

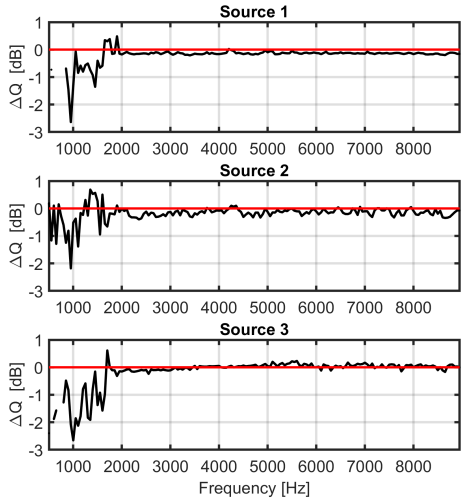

(a) CMF-OMPCV

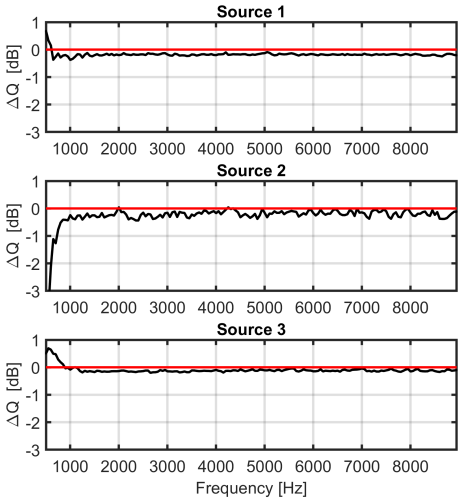

(b) CMF-LassoLars $\lambda = 10^{-6}$

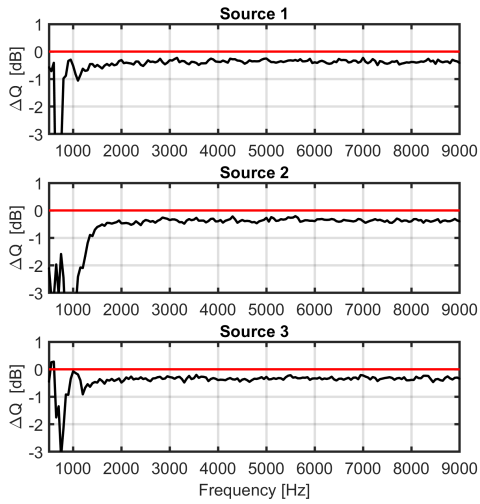

(c) CMF-IRLS $p = 1$

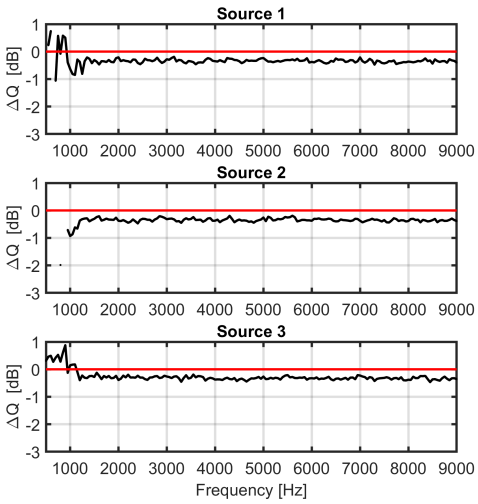

(d) CMF-IRLS $p = 0.9$

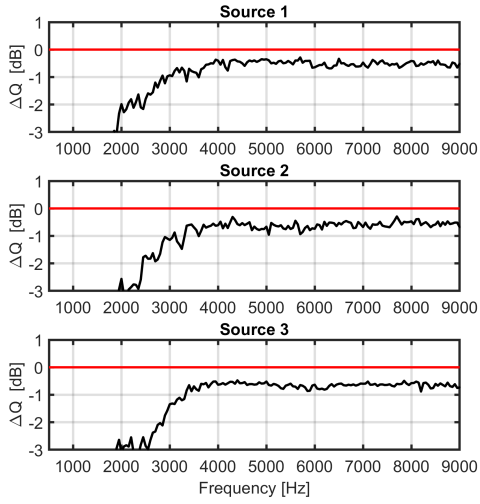

(e) ESM-IRLS $p = 1$

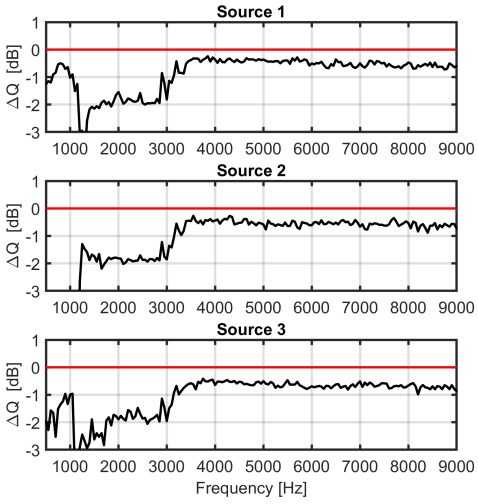

(f) ESM-IRLS $p = 0.9$

Figure 6: Reconstructed spectra of sources

3.2 Experimental data

The second test case is a real experiment conducted in the aeroacoustic wind tunnel at Brandenburg University of Technology [13]. A NACA 0012 airfoil is positioned in an open jet of diameter 0.2 m and core velocity 50 m/s. The airfoil has a span of 0.28 m and a chord length of 0.25 m. The boundary layer tripping was realized with a 2.5mm anti-slip tape applied at 10% of the chord both on the suction and the pressure side. The array utilized has 56 microphones and a diameter $D = 1.3$ m; it was placed 0.715 m above the airfoil with respect to the array. Figure 7 shows the position of the airfoil and the nozzle. The volume of interest has dimensions $Dx = 1.1$ m, $Dy = 1.2$ m and $Dz = 0.8$ m and is discretized with a regular grid of 2 cm of resolution. The resulting number of points is 140.056. Data were sampled at 51200 samples/s and the CSM is estimated averaging 4000 blocks of 1024 samples (overlap 50%) using Hanning window. The frequency resolution obtained is 50 Hz. The eigenvalues of CSM, for each band of interest, are depicted in Fig. 8, ESM is applied to the first 10 eigenmodes of each band. Also in this test case the sound propagation through the flow field is calculated using *Acoular* OpenJet environment. In this scenario the regularization parameter for LassoLars solver is set to 10^{-9}.

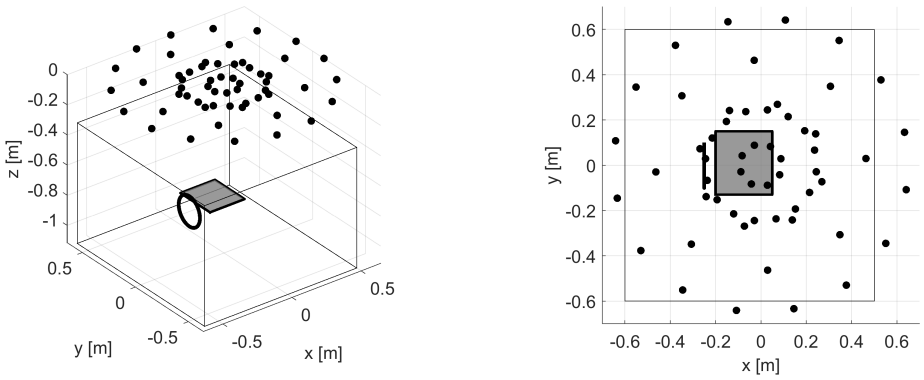

Figure 7: Measurement setup

At 4 kHz and 8 kHz, all methods provide reliable results except the CMF-LassoLars approach. Indeed, the latter produces empty results for these bands. This is surely due to the choice of the regularization parameter. Authors are still trying to link this behaviour a correct choice of the latter. Trailing-edge noise generation mechanism is clearly visible as a linear source as well as the interaction between leading-edge and shear layer. At 1 kHz, CMF-IRLS and ESM-IRLS with $p = 1$ produce maps where the trailing-edge noise is evident, while maps obtained by CMF-OMPCV, CMF-LassoLars and ESM-IRLS with $p = 0.9$ may be misleading. At 2kHz a difference between CMF and ESM is visible. Indeed, CMF identifies only sources at trailing-edge, while ESM can reconstruct also sources at leading-edge. This is due to the eigenmode decomposition of CSM operated in ESM. In fact, the first two eigenmodes are related to trailing-edge noise while the following three are related to leading-edge noise. The regularization mechanism in CMF tends to suppress sources with less power because of the noisy environment, while ESM is still able to identify those sources.

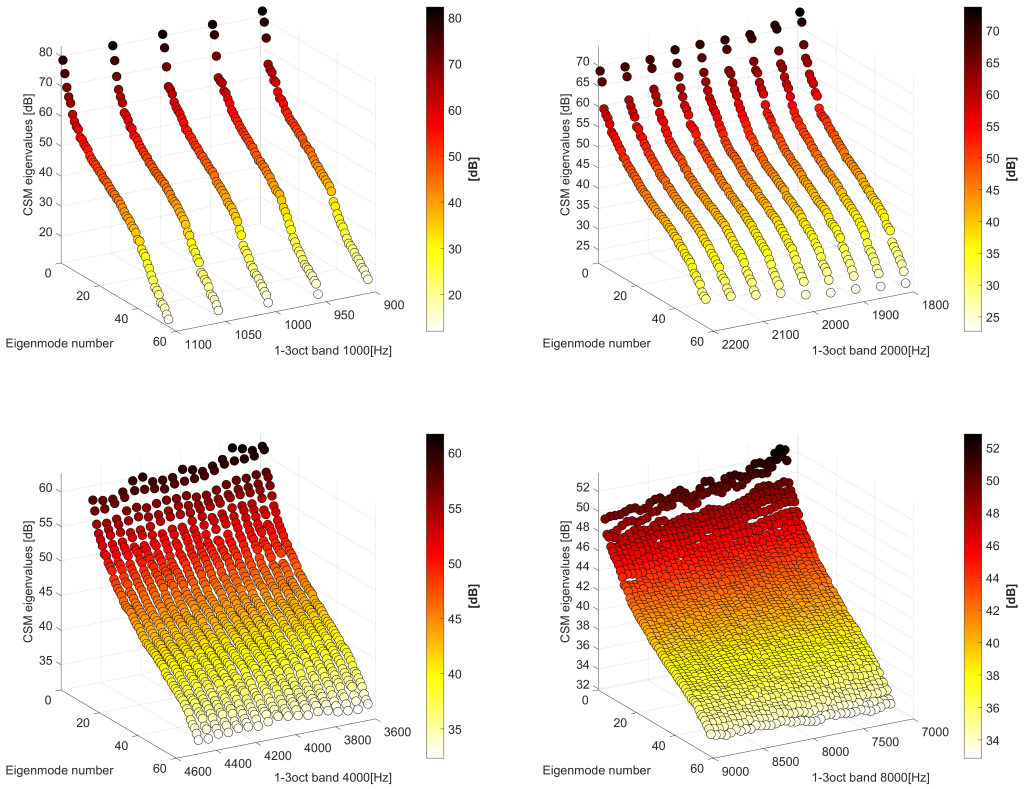

Figure 8: Eigenvalues of CSM

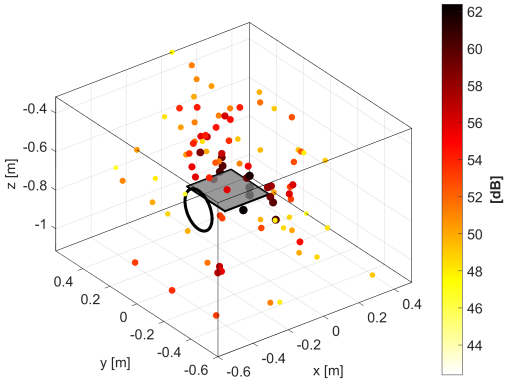

(a) CMF-OMPCV

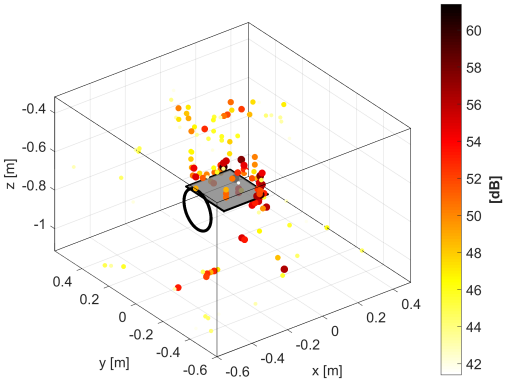

(b) CMF-LassoLars $\lambda = 10^{-9}$

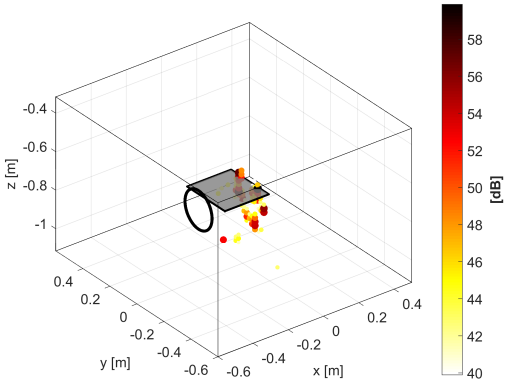

(c) CMF-IRLS $p = 1$

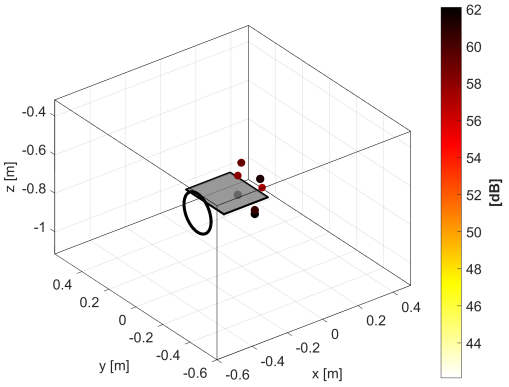

(d) CMF-IRLS $p = 0.9$

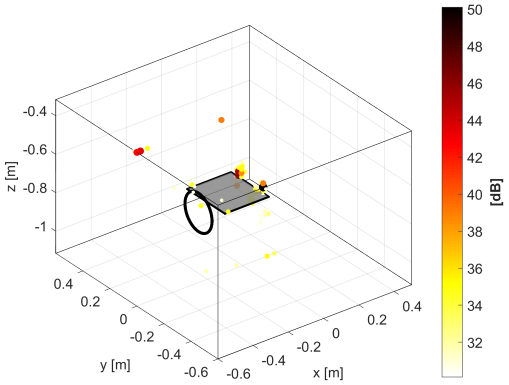

(e) ESM-IRLS $p = 1$

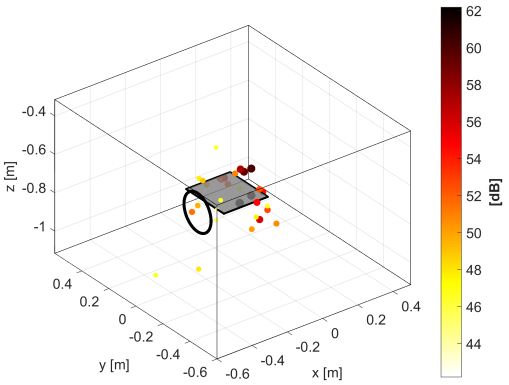

(f) ESM-IRLS $p = 0.9$

Figure 9: 1000 Hz 1/3-octave band (He ≈ 3.4 - 4.1)

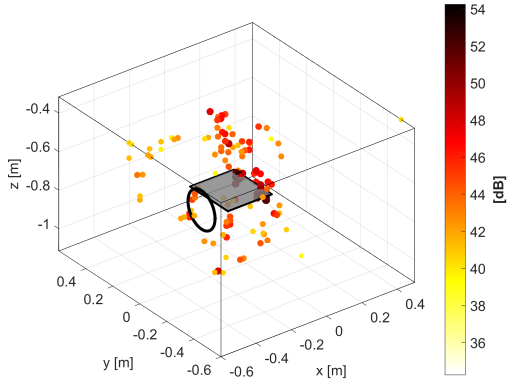

(a) CMF-OMPCV

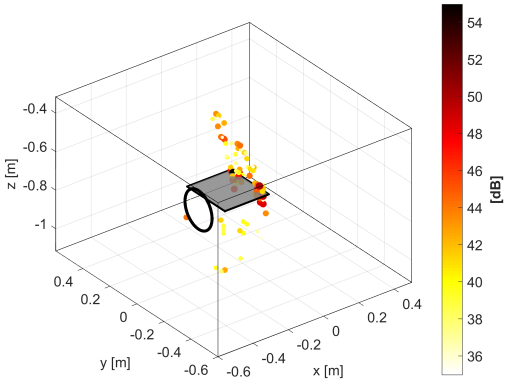

(b) CMF-LassoLars $\lambda = 10^{-9}$

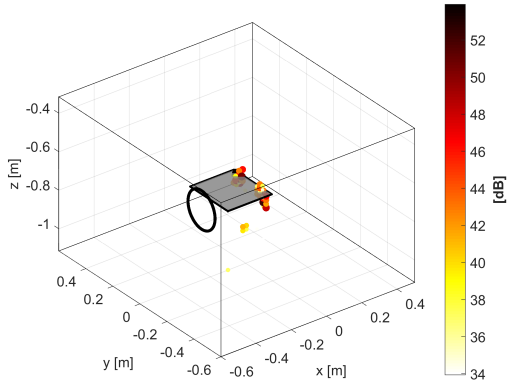

(c) CMF-IRLS $p = 1$

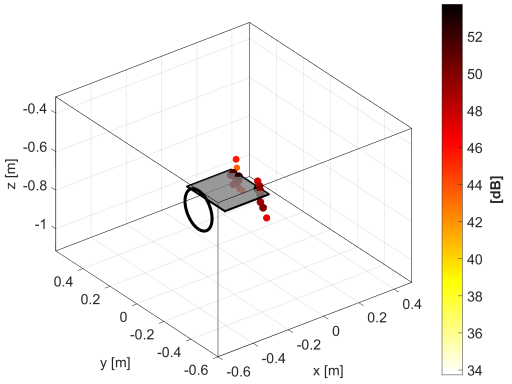

(d) CMF-IRLS $p = 0.9$

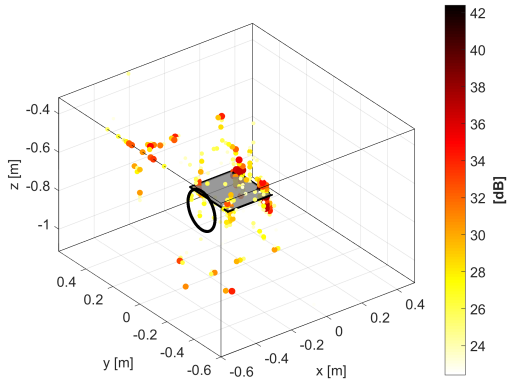

(e) ESM-IRLS $p = 1$

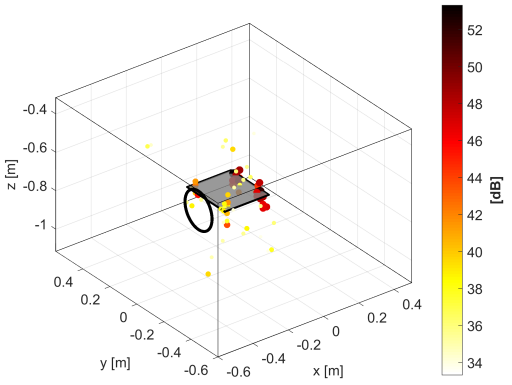

(f) ESM-IRLS $p = 0.9$

Figure 10: 2000 Hz 1/3-octave band (He ≈ 6.7 - 8.2)

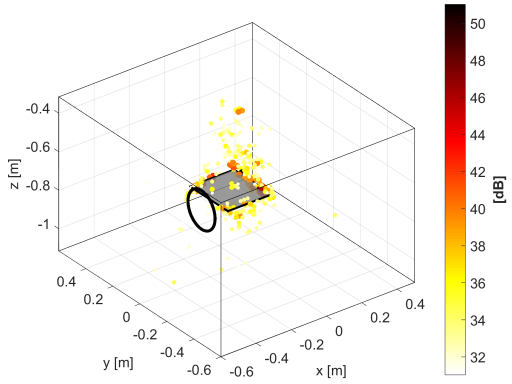

(a) CMF-OMPCV

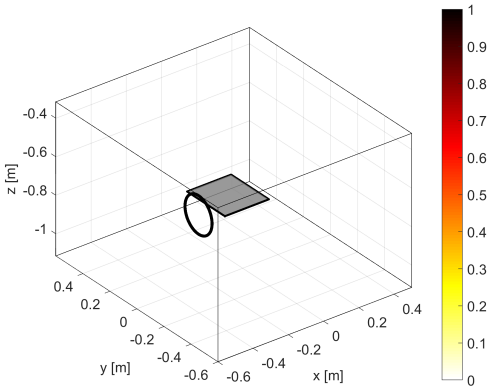

(b) CMF-LassoLars $\lambda = 10^{-9}$

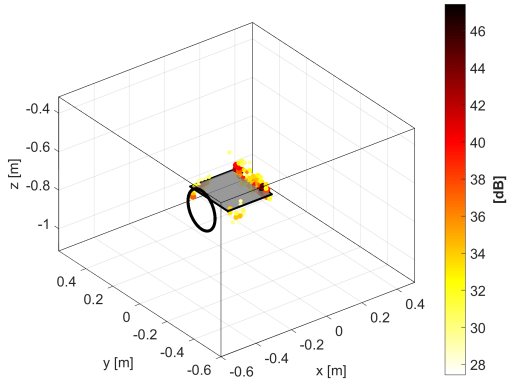

(c) CMF-IRLS $p = 1$

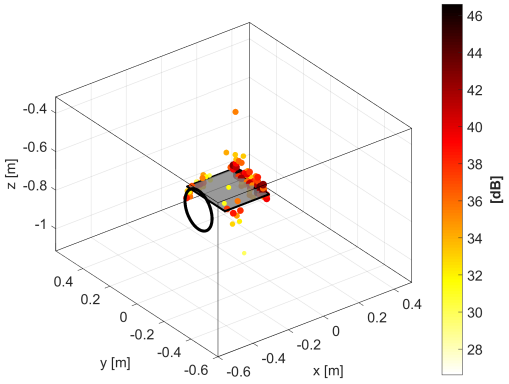

(d) CMF-IRLS $p = 0.9$

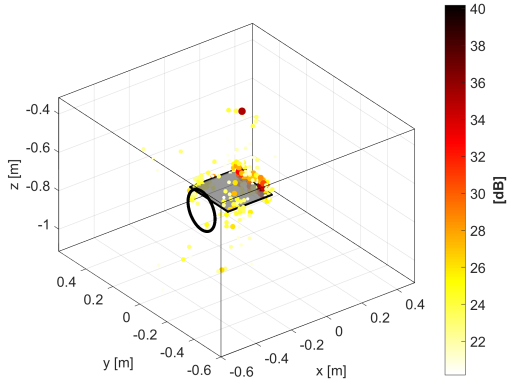

(e) ESM-IRLS $p = 1$

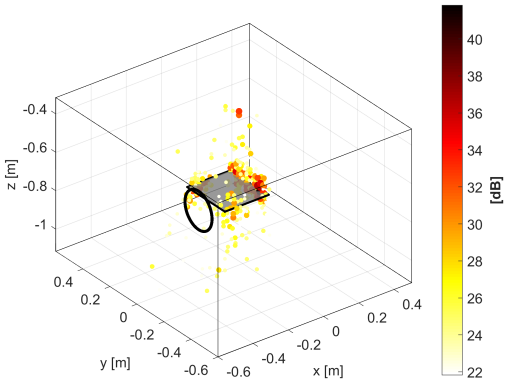

(f) ESM-IRLS $p = 0.9$

Figure 11: 4000 Hz 1/3-octave band (He ≈ 13.5 - 16.7)

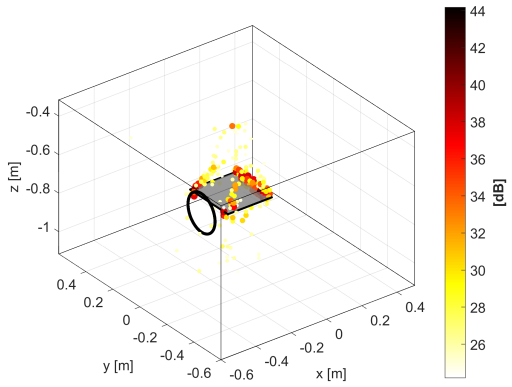

(a) CMF-OMPCV

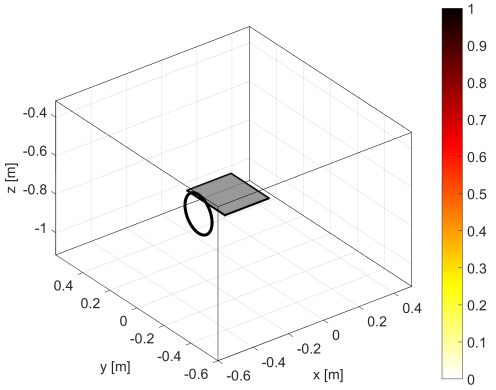

(b) CMF-LassoLars $\lambda = 10^{-9}$

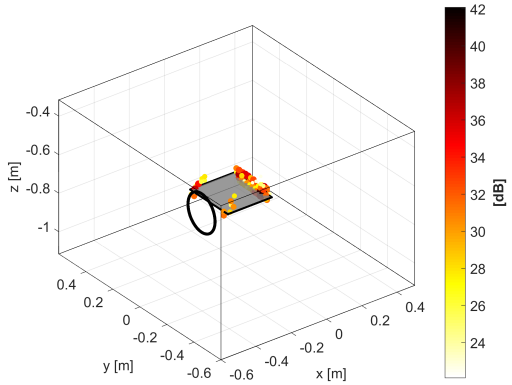

(c) CMF-IRLS $p = 1$

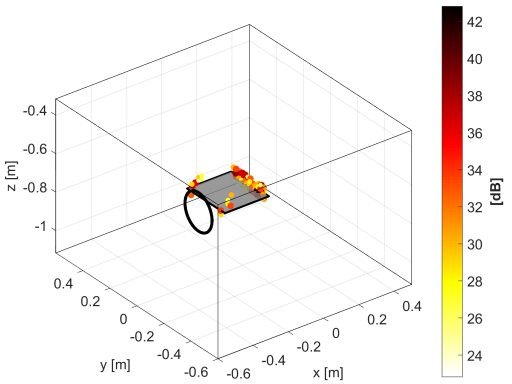

(d) CMF-IRLS $p = 0.9$

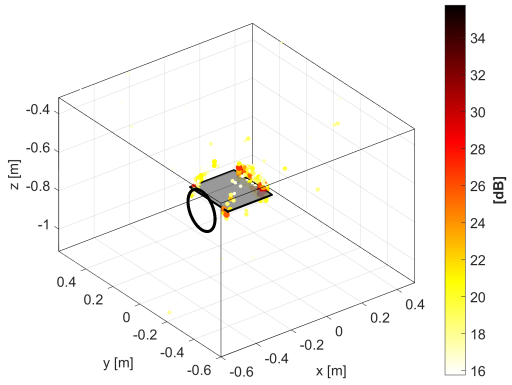

(e) ESM-IRLS $p = 1$

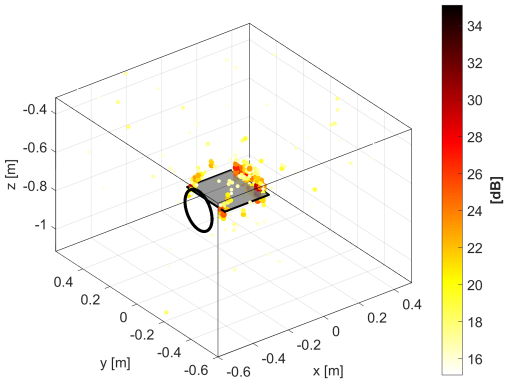

(f) ESM-IRLS $p = 0.9$

Figure 12: 8000 Hz 1/3-octave band (He ≈ 26.8 - 33.5)

4 CONCLUSIONS

A study on three-dimensional volumetric mapping with inverse methods has been presented in this paper. The use of a single planar array makes the source localization task very difficult because additional issues must be faced with respect to standard acoustic imaging on surfaces. The strategies described in this paper produced accurate results in this challenging context, in particular Bayesian approach combined with IRLS demonstrated to be a robust approach. Another positive aspect of these techniques is that they do not require any additional hardware or any sort of modification to typical measurement setup, therefore they can be applied also to measurement data already acquired for standard acoustic mapping.

REFERENCES

[1] "Acoular acoustic testing and source mapping software.", 2018. URL `http://www.acoular.org`.

[2] "Benchmarking array analysis methods.", 2018. URL `https://www.b-tu.de/fg-akustik/lehre/aktuelles/arraybenchmark`.

[3] J. Antoni. "A bayesian approach to sound source reconstruction: Optimal basis, regularization, and focusing." *The Journal of the Acoustical Society of America*, 131(4), 2873–2890, 2012. doi:10.1121/1.3685484.

[4] P. Boufounos, M. F. Duarte, and R. G. Baraniuk. "Sparse signal reconstruction from noisy compressive measurements using cross validation." In *2007 IEEE/SP 14th Workshop on Statistical Signal Processing*. IEEE, 2007. doi:10.1109/ssp.2007.4301267.

[5] T. F. Brooks and W. M. Humphreys, Jr. "A deconvolution approach for the mapping of acoustic sources (DAMAS) determined from phased microphone array." *Journal of Sound and Vibration*, 294(4-5), 856–879, 2006. doi:10.1016/j.jsv.2005.12.046.

[6] T. F. Brooks and W. M. Humphreys, Jr. "Extension of DAMAS Phased Array Processing for Spatial Coherence Determination (DAMAS-C)." In *12th AIAA/CEAS Aeroacoustics Conference, Cambridge, Massachusetts, May 8-10, 2006*. 2006.

[7] R. Chartrand and W. Yin. "Iteratively reweighted algorithms for compressive sensing." In *2008 IEEE International Conference on Acoustics, Speech and Signal Processing*. IEEE, 2008. doi:10.1109/icassp.2008.4518498.

[8] I. Daubechies, R. DeVore, M. Fornasier, and C. S. Güntürk. "Iteratively reweighted least squares minimization for sparse recovery." *Communications on Pure and Applied Mathematics*, 63(1), 1–38, 2010. doi:10.1002/cpa.20303.

[9] J. Hadamard. "Sur les problèmes aux dérivés partielles et leur signification physique." *Princeton University Bulletin*, 13, 49–52, 1902.

[10] P. C. Hansen. "The discrete picard condition for discrete ill-posed problems." *BIT*, 30(4), 658–672, 1990. doi:10.1007/bf01933214.

[11] P. C. Hansen. "Regularization tools: A matlab package for analysis and solution of discrete ill-posed problems." *Numerical algorithms*, 6(1), 1–35, 1994. doi:10.1007/BF02149761.

[12] P. C. Hansen. *Rank-deficient and discrete ill-posed problems*. SIAM Monographs on Mathematical Modeling and Computation. Society for Industrial and Applied Mathematics (SIAM), Philadelphia, PA, 1998. ISBN 0-89871-403-6. Numerical aspects of linear inversion.

[13] G. Herold, T. F. Geyer, and E. Sarradj. "Comparison of inverse deconvolution algorithms for high-resolution aeroacoustic source characterization." In *23rd AIAA/CEAS Aeroacoustics Conference*. American Institute of Aeronautics and Astronautics, 2017. doi: 10.2514/6.2017-4177.

[14] G. Herold, E. Sarradj, and T. Geyer. "Covariance matrix fitting for aeroacoustic application." In *Fortschritte der Akustik - DAGA*. 2013.

[15] G. Herold, E. Sarradj, and T. Geyer. "Covariance matrix fitting for aeroacoustic application." In *Fortschritte der Akustik - AIA-DAGA 2013*, pages 1926 – 1928. 2014.

[16] Y. Kim and P. Nelson. "Optimal regularisation for acoustic source reconstruction by inverse methods." *Journal of Sound and Vibration*, 275(3-5), 463–487, 2004. doi: 10.1016/j.jsv.2003.06.031.

[17] G. H. Koopmann, L. Song, and J. B. Fahnline. "A method for computing acoustic fields based on the principle of wave superposition." *The Journal of the Acoustical Society of America*, 86(6), 2433–2438, 1989. doi:10.1121/1.398450.

[18] Q. Leclère. "Acoustic imaging using under-determined inverse approaches: Frequency limitations and optimal regularization." *Journal of Sound and Vibration*, 321(3-5), 605–619, 2009. ISSN 0022-460X. doi:http://dx.doi.org/10.1016/j.jsv.2008.10.022. URL `http://www.sciencedirect.com/science/article/pii/S0022460X08008729`.

[19] Q. Leclère, A. Pereira, C. Bailly, J. Antoni, and C. Picard. "A unified formalism for acoustic imaging techniques: illustrations in the frame of a didactic numerical benchmark." In *Proceedings on CD of the 6th Berlin Beamforming Conference, 29 February-1 March 2016*. 2016. ISBN 978-3-942709-15-6. URL `http://www.bebec.eu/Downloads/BeBeC2016/Papers/BeBeC-2016-D5.pdf`.

[20] F. Ning, J. Wei, L. Qiu, H. Shi, and X. Li. "Three-dimensional acoustic imaging with planar microphone arrays and compressive sensing." *Journal of Sound and Vibration*, 380, 112–128, 2016. doi:10.1016/j.jsv.2016.06.009.

[21] B. Oudompheng, A. Pereira, C. Picard, Q. Leclère, and B. Nicolas. "A theoretical and experimental comparison of the iterative equivalent source method and the generalized inverse beamforming." In *5th BeBec*. 2014. ISBN 978-3-942709-12-5. URL `http://bebec.eu/Downloads/BeBeC2014/Papers/BeBeC-2014-12.pdf`.

[22] S. P. "Clean based on spatial source coherence." *International Journal of Aeroacoustics*, 6(4), 357–374, 2007. URL http://dx.doi.org/10.1260/147547207783359459.

[23] T. Padois and A. Berry. "Two and three-dimensional sound source localization with beamforming and several deconvolution techniques." *Acta Acustica united with Acustica*, 103(3), 392–400, 2017. doi:10.3813/aaa.919069.

[24] T. Padois, O. Robin, and A. Berry. "3d source localization in a closed wind-tunnel using microphone arrays." In *19th AIAA/CEAS Aeroacoustics Conference*. American Institute of Aeronautics and Astronautics (AIAA), 2013. doi:10.2514/6.2013-2213.

[25] Y. C. Pati, R. Rezaiifar, and P. S. Krishnaprasad. "Orthogonal matching pursuit: Recursive function approximation with applications to wavelet decomposition." In *in Conference Record of The Twenty-Seventh Asilomar Conference on Signals, Systems and Computers*, pages 1–3. 1993.

[26] F. Pedregosa, G. Varoquaux, A. Gramfort, V. Michel, B. Thirion, O. Grisel, M. Blondel, P. Prettenhofer, R. Weiss, V. Dubourg, J. Vanderplas, A. Passos, D. Cournapeau, M. Brucher, M. Perrot, and E. Duchesnay. "Scikit-learn: Machine learning in python." *J. Mach. Learn. Res.*, 12, 2825–2830, 2011. ISSN 1532-4435. URL http://dl.acm.org/citation.cfm?id=1953048.2078195.

[27] A. Pereira. *Acoustic imaging in enclosed spaces*. Ph.D. thesis, INSA de Lyon, 2014.

[28] A. Pereira, J. Antoni, and Q. Leclère. "Empirical bayesian regularization of the inverse acoustic problem." *Applied Acoustics*, 97, 11–29, 2015. doi:10.1016/j.apacoust.2015.03.008.

[29] A. Pereira and Q. Leclère. "Improving the Equivalent Source Method for noise source identification in enclosed spaces." In *18th International Congress on Sound and Vibration (ICSV 18)*, page R31. Brazil, 2011. URL https://hal.archives-ouvertes.fr/hal-01006201.

[30] F. Presezniak, P. Zavala, G. Steenackers, K. Janssens, J. Arruda, W. Desmet, and P. Guillaume. "Acoustic source identification using a generalized weighted inverse beamforming technique." *Mechanical Systems and Signal Processing*, 32, 349–358, 2012. doi:10.1016/j.ymssp.2012.06.019. URL https://www.scopus.com/inward/record.uri?eid=2-s2.0-84865043449&partnerID=40&md5=b9885cc80559a22f6cf8d461d17e6447, cited By 5.

[31] R. Rubinstein, M. Zibulevsky, and M. Elad. "Efficient implementation of the k-svd algorithm using batch orthogonal matching pursuit."

[32] E. Sarradj. "Three-dimensional acoustic source mapping." In *4th Bebec*. 2012.

[33] E. Sarradj. "Three-dimensional acoustic source mapping with different beamforming steering vector formulations." *Advances in Acoustics and Vibration*, 2012(292695), 1–12, 2012. doi:10.1155/2012/292695.

[34] E. Sarradj and G. Herold. "A python framework for microphone array data processing." *Applied Acoustics*, 116, 50–58, 2017. doi:10.1016/j.apacoust.2016.09.015.

[35] E. Sarradj, C. Schulze, and A. Zeibig. "Identification of Noise Source Mechanisms using Orthogonal Beamforming." In *Noise and Vibration: Emerging Methods*. 2005.

[36] T. Suzuki. "L1 generalized inverse beam-forming algorithm resolving coherent/incoherent, distributed and multipole sources." *Journal of Sound and Vibration*, 330, 5835–5851, 2011. doi:10.1016/j.jsv.2011.05.021.

[37] R. Tibshirani, I. Johnstone, T. Hastie, and B. Efron. "Least angle regression." *The Annals of Statistics*, 32(2), 407–499, 2004. doi:10.1214/009053604000000067.

[38] A. N. Tikhonov. "Solution of incorrectly formulated problems and the regularization method." *Soviet Math. Dokl.*, 4, 1035–1038, 1963.

[39] T. Yardibi, J. Li, P. Stoica, and L. N. Cattafesta. "Sparsity constrained deconvolution approaches for acoustic source mapping." *The Journal of the Acoustical Society of America*, 123(5), 2631–2642, 2008. doi:http://dx.doi.org/10.1121/1.2896754. URL `http://scitation.aip.org/content/asa/journal/jasa/123/5/10.1121/1.2896754`.

[40] P. Zavala, W. De Roeck, K. Janssens, J. Arruda, P. Sas, and W. Desmet. "Generalized inverse beamforming with optimized regularization strategy." *Mechanical Systems and Signal Processing*, 25(3), 928–939, 2011.